Prediction of wind farm wake and output power using generative adversarial network and convolutional neural network

Jian Chen*[1], Chongyang Yu[1], Zhongyun Xu[2], Ruiyang He[3], Chun Li[1], Wanfu Zhang[1], Ying Wang[1]

[1]School of Energy and Power Engineering, University of Shanghai for Science and Technology, Shanghai, 200093, PR China

[2]Jiangnan Shipyard(Group) Co.,Ltd, Shanghai, 201913, PR China

[3]School of Engineering, Cardiff University, Cardiff CF24 3AA, UK

*Corresponding author Email: 09900589R@connect.polyu.hk

Abstract

Wake and output power prediction of wind turbine is critical for the wind farm layout optimization. Previous studies used analytical wake models (AWMs) and computational fluid dynamics (CFD) methods to fulfill this prediction. However, these methods either exhibit inadequate prediction accuracy or need excessive computational demands during prediction processes. Thus, a novel wind farm prediction system is established using the full-model CFD simulation and a surrogate modeling method based on convolutional neural networks (CNNs) and generative adversarial networks (GANs) to ensure the fidelity and efficiency of the prediction. By containing an incoming speed distribution generator module (G_{in}), a wake distribution generator model (G_w), a rotational speed prediction module (R), and a power prediction module (P), this system can predict high-dimensional incoming data, the rotational speed, power output, and 3D wake fields. The system uses the incoming wind speed (V_{in}) and turbulence intensity (TI) to determine the optimal placement of turbines in the wind field. The G_{in}, R , G_w and P module are validated through high-resolution experimental and computational data. The system is applied to a tandem wind farm and the Horns Rev 1 wind farm. The predicted data shows satisfactory agreement with high-resolution experimental and computational data, fully validating the robustness and generalization capability of the system. The proposed prediction system is of great engineering significance for optimizing wind farm layout.

Keywords: Full-model CFD simulation; Convolutional neural network; Generative adversarial network; Wake

prediction; Output power

1 Introduction

Wind energy is widely invested due to its vast and wide reversion. To fully utilize the wind energy resources and improve the economics of wind power generation, wind turbines are usually installed together to form large wind farms [1]. The power output and wake of the wind turbine are two critical factors for wind farm design [2] and the wake significantly affects the performance of the downstream turbine [3]. Therefore, predicting the output power and wake characteristics of wind turbines is crucial for the layout optimization of wind farm and maximization of the overall power generation [4]. Reliable prediction can not only help wind farms to improve the rate of wind power consumption, but also increase the economic returns of wind farms[5].

Nowadays the dominated methods for the wind turbine wake modeling include AWMs and CFD simulation. The AWMs is widely used because of its simplicity and rapidity of calculation. Jensen model is a simple engineering wake model firstly proposed [6], which is a one-dimensional (1D) model. Jensen regards the wake of a downstream wind turbine as a turbulent wake and assumes that the radius size of the wake region expands linearly with the downstream distance, and the degree of velocity reduction depends only on the distance of the downstream region from the rotor. The effect of blade shedding vortices on the near-field flow field is neglected to simplify the model. Frandsen et al. [7] proposed another 1D model, which is similar in velocity distribution to the Jensen model, also following a "hat" distribution. The key difference is that it treats the entire cylindrical region behind the rotor as a control volume and uses momentum theory to derive the conclusions. Gao et al. [8] employed the two-dimensional (2D) model for wind farm optimization and compared its results with those of the original 1D model. They found that the 2D model provided results that were more accurate in predicting the wind farm's power generation efficiency compared to the 1D model. In addition, some researchers have suggested that the mixed installation of different types of wind turbines with different hub heights and diameters to establish non-uniform wind farms can help to increase the overall power output and reduce the cost-benefit ratio [9], and the layout optimization of non-uniform wind farms needs to consider the heights of different wind turbines. Therefore, current research is focused on establishing a three-dimensional (3D) wake model that accounts for the effect of height [10]-[13]. Gao et al [14] added the wind shear effect to the Jensen-Gaussian model to make it 3D and expressed the wind speed through an exponential function to improve the prediction accuracy in the vertical direction. However, the analytical model has obvious drawbacks because it usually lacks of accuracy.

To assess wake interactions between wind turbines and capture more accurate wake characteristics, the actuator disk method (ADM) and the actuator line method (ALM) are commonly employed for CFD simulations of wind

turbine rotors. The ADM simplifies the rotor into a virtual disk, significantly reducing the mesh requirements and computational resources. Khan et al. [15] used the ADM to optimize the scheduling of a nine-turbine wind farm. Liu et al. [16] used a large eddy simulation (LES) combined with the ADM to study the positive effect of wind deflectors on the overall flow field and power enhancement of wind farms. Onal et al. [17] employed the ALM to investigate wake interactions and power production effects in a tandem wind turbine configuration, assessing the influence of turbulent incoming conditions on wake dynamics. Wang et al. [18] used the ALM to simulate the yaw operation of wind turbines and observed the asymmetric counter-rotating phenomenon in the wake of yawed turbines caused by the periodic variation of tip vortex. Steven et al. [19] compared LES using ALM and ADM and found that both methods produced reasonably accurate far-field wake data. However, the ALM exhibits sensitivity to mesh resolution and struggles to accurately resolve complex 3D wake effects, while the ADM inherently neglects blade geometric details and unsteady flow features through spatial averaging. Both approaches may underestimate the influence of localized flow separation, leading to compromised accuracy in aerodynamic load predictions. Therefore, ALM and ADM are still not accurate enough.

The full-model CFD simulation differs from the ALM and ADM in that real wind turbine geometry is used to build the computational domain. It can better capture the flow at the blade surface and wake development, making it widely used in advanced research9. Zhou et al. [20] investigated the effects of turbulence and wind shear on a floating offshore wind turbine using a full-model CFD method and found that turbulent winds resulted in faster wake spreading. Fu et al. [21] simulated the longitudinal rocking conditions of a model floating offshore wind turbine using an overlapping grid approach. Miao et al. [22] simulated the flow field conditions of a yawed tandem wind farm using a full-model CFD method and found that the intentional yawing of the upstream wind turbine can increase the total power output of the wind farm. Ye et al. [23] employed full-model CFD simulations to replicate the wind turbine wake results from wind tunnel experiments and investigate the influence of rotating blades on the deflection of tower wakes. It showed that full-model CFD simulation can accurately capture the complex aerodynamic characteristics, turbulence effects, blade details and turbine interactions. However, full model CFD simulation is time-consuming. The disadvantage of this can be overcome by combining full-model CFD simulation with machine learning techniques.

In recent years, with the rapid development of artificial intelligence, a series of machine learning techniques have been applied to wind turbine research including Graph Neural Networks (GNN), Artificial Neural Networks (ANN), Long Short-Term Memory (LSTM), Visual Transformer (ViT), CNN. Li et al. [24] proposed a structure based on GNN combined with residual network to accurately predict the wind turbine wake flow field under

different incoming conditions and yaw angles, which is less sensitive to the transition smoothing of the data and has a more flexible framework with higher generalizability compared to the underlying network structure. Sun et al. [25] developed an ANN power model for calculating the total power of yawed wind turbine based on the ANN modeling and field data collected from Supervisory Control and Data Acquisition (SCADA) to calculate the total power of a yawing wind turbine. The model is then applied to optimize the yaw angle of the wind turbine. Zhang and Zhao [26] used LSTM to predict the reduced-dimensional dynamic wake field in the hub-height horizontal plane. The results show that the combined model is like high-fidelity numerical simulations and is effective in capturing the main features of the non-constant wind turbine wake. Li et al. [27] used the state-of-the-art Transformer model to predict the power generation of individual wind turbines in a wind farm. However, ANNs, LSTMs, and CNNs [28] are discriminative models that primarily focus on learning the mapping relationships between input and output data, without explicitly capturing the underlying physical processes governing the dataset. Consequently, these models require a substantial volume of training data to achieve satisfactory results. Previous studies have used low-precision data from AWMs, ADM or ALM as training or test data. Low accuracy data reduce the perdition ability of the machine-learning based wake models. Thus, a high-precision dataset is crucial for the machine-learning based wake models. This reliance on large and accuracy datasets significantly increases computational costs, posing a challenge for practical applications.

To solve the problem of the large amount of training data required for the models, some recent studies have used GAN generators to generate part of the training data, thus significantly reducing the computational expense of CFD. Zhang and Zhao [29] proposed a deep convolutional conditional generative adversarial network (CGAN), which serves as a popular generative model for simulating the corresponding flow parameters for a non-constant wind turbine wake. The dataset used for model training is built by high-fidelity numerical simulations, and the validation results show that the predicted data are in good agreement with the high-fidelity data. Li et al. [30] integrate the Transformer module into the CGAN, use a combination of analytical and numerical data generation methods, establish a large-scale wake flow database, and employ a pre-training-fine-tuning strategy to increase the efficiency of model training and enhance the prediction performance, and use a pre-training-fine-tuning strategy to improve the model training efficiency. It is expected that GANs are going to further applied on wake flow studies in the future. However, the current research of machine learning methods in wind farm prediction still faces some limitations, which are listed below:

(1) Datasets of previous studies are usually obtained from Jensen model, ALM or ADM method. However, the accuracy of the training dataset is very important for deep learning. An inaccurate dataset often leads to the

impairment of the generalization ability in model training.

(2) The majority studies used low-dimensional incoming data to predict the wake and power output. It has been suggested that there are significant differences in the spatial representation of high-dimensional incoming data, which can be used to capture more precise details of the wake distribution [29].

(3) Although GAN have been predominantly employed in prior wake modeling research, CGAN architectures have the training instability due to fundamentally unidirectional mapping paradigm and potential spatial irreversibility.

(4) A prediction system that can quickly and accurately predict multiple key elements in a wind farm, such as the incoming flow field, TI, wake velocity, the rotational speed of wind turbines, and the output power, is crucial for achieving the optimization of wind farm layout and the cooperative control of wind turbines within the wind farm.

To improve the accuracy of the training data, we use the full-model CFD simulation results as the database. The high-precision inflow data gained from CFD is used to train a transposed convolution incoming speed distribution generator which is used to capture more accurate details of the wake distribution. The incoming speed distribution generator is trained using CGAN to obtain high-dimensional incoming data by inputting V_{in} and TI. The cycle generative adversarial network (Cycle GAN) was used to train the 3D wake models to improve the training accuracy and stability. Meanwhile, a complete wind farm prediction system with independent modules has been proposed for wind farm layout optimization.

The main contributions and innovations of this paper are as follows:

(1) To stabilize the model training and enhance the prediction accuracy, high-fidelity full-model CFD simulation are used to establish the database of model training.

(2) The incoming speed distribution generator trained by high-precision CFD simulation data and CGAN can generate high-dimensional incoming data based on V_{in} and TI, eliminating the need for non-uniform high-dimensional data from light detection and ranging (LIDAR), AWMs or CFD.

(3) To improve the rationality of the model results and stabilize the training results, a modeling framework of Cycle GAN is proposed. This system can achieve backward prediction from the incoming flow field to the wake flow field, it can also realize the forward physical field reconstruction from the wake flow field to the incoming flow field, thus establishing a cyclic data flow architecture.

(4) To achieve the optimization of the wind farm layout and the coordinated control of the wind turbines in the

wind farm quickly and accurately, an integrated system has been established using a deep learning approach V_{in} and TI as inputs to obtain high-dimensional incoming flow data which can be used to obtain the wind turbine rotational speed, power output, and 3D wake at different axial distances. A novel momentum compensation is used to correct the downstream turbine wake velocity, optimizing far wake recovery prediction.

The rest of the paper is organized as follows: Section 2 describes the CFD simulation method, data collection method, wake field fitting method and wind farm prediction method. Thereafter, the dataset validation, the discussion of the results of the training of the model, the assessment of the performance of the wake flow fitting, and the validation of the model against the predicted values using real wind farms are given in Section 3. Finally, Section 4 summarizes the main conclusions.

2 Methods

2.1 CFD simulation strategies

2.1.1 Geometric modeling of wind turbines

The HAWT model selected for this paper is a 5 MW wind turbine developed by the National Renewable Energy Laboratory (NREL) [31]. As stated in the reference [32], the removal of tower, nacelle, and other auxiliary mechanisms from the wind turbine model has a minimal impact on the simulation results. Therefore, this paper uses the wind turbine model without the tower and nacelle to enhance computational efficiency and maintain the simulation fidelity. The main parameters of the wind turbine are presented in Table 1.

Table 1 NREL 5MW wind turbine parameters

Item	Value
Roto diameter (m)	126
Hub height (m)	90
Rated wind speed (m/s)	11.4
Roto rotational speed (RPM)	12.1
Blade number	3

2.1.2 Mesh and boundary conditions

As shown in Fig. 1, the computational domain of the wind farm is divided into two parts: a rotating domain and a stationary domain. The stationary domain is a rectangular body with dimension of 4D (x) × 3D (y) ×18D (z), where D is the turbine rotor diameter. The wind turbine is located within the cylindrical rotating domain. The hub center of wind turbine positioned at 2D from both the left and right interfaces of rotating domain. The blockage

ratio for this configuration is 6.5% to ensure the full flow development[32]. The center of the rotating domain is 3D from the inlet to allow the full development of the inlet flow. A steady-state 3D RANS simulation is performed using an implicit solver, and the SIMPLE algorithm employed for the pressure-velocity coupling. The discretization scheme uses the second-order upwind scheme. The inlet is set as a velocity inlet with velocity (V) range from 5 m/s to 11.4 m/s, and the inlet TI ranges from 5% to 25%. Table 2 indicates the selection of rotational speed of the wind turbine rotor for different ranges of V_{in}, the rotational speed (n) of the rotating domain is adjusted according to wind speeds shown in Table 2. The outlet boundary condition sets as a pressure outlet with an outlet pressure of 0 Pa. The left and right surfaces are symmetry boundaries. The surfaces between the rotating and stationary domains are set as interface boundaries to fulfill the sliding mesh method.

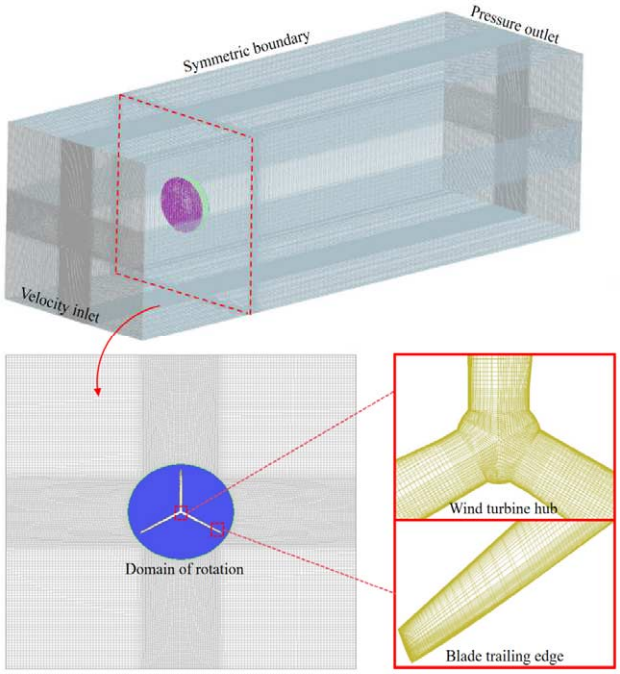

Fig. 1. Fluid domain mesh model

Table 2 Velocity and corresponding rotational speed

V(m/s)	[5, 6)	[6, 7)	[7, 8)	[8, 9)	[9, 10)	[10, 11)	[11,11.4)
Rotational speed (RPM)	7.4	8.0	8.6	9.2	10.3	11.4	12.1

R level	1	2	3	4	5	6	7

Since grid density affects the accuracy of CFD calculation results, inaccurate CFD data can impact the precision of the model. Therefore, it is necessary to study grid independence. Under rated wind speed and rated rotational speed conditions, an independence analysis was conducted on the total number of grids in the model, with the results shown in the Fig. 2. The grid independence verification indicates that coarse wind turbine blade grids result in underestimated predicted power. When the total number exceeds 10 million, the numerical values tend to stabilize, with errors around 2%.

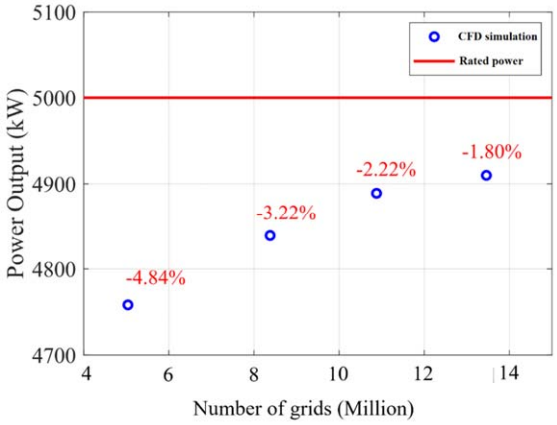

Fig. 2. Grid independence verification

The quality of the mesh used in the computational domain is of great importance to the accuracy of the CFD simulation results. The geometric model of the wind turbine, constructed using SolidWorks, is imported into ICEM to generate the structured meshing. The mesh is refined in wind turbine downstream region to capture the wake features. To ensure the y+ value is equal to 1, 20 boundary layers meshes are added on the wind turbine blades with the first layer height is 8×10^{-5} m and the growth rate of 1.2. The number of meshes in the rotational domain and whole computational domain is 7.26 million and 10.88 million, respectively.

2.2 Training and testing data collection method

The training and testing data for deep learning model are gained from the full-model CFD simulation including incoming speed, wake velocity, wake TI, and output power of the wind turbine. Fig. 3 shows the sampling points for the training and testing data. For incoming speed, the sampling points are located at the 0.1D position in front of the wind turbine. Since the wind turbine rotor exhibits a rotationally symmetric pattern, this paper used three lines C1, C2, C3 separated by 120° to represent the incoming data. 13 sampling points are set for each line. For wake distribution, starting from 3D, 13 slices are taken with interval of 1D along the z-direction. Two crossed lines

is selected in each slice for data sampling. Each line has 17 sampling points. 13 sampling points are located in the wind turbine region, and 4 sampling point are outside of the wind turbine region. Each sampling point collects instantaneous velocity value at every time step. The instantaneous velocity $\overline{U}$ can be calculated by Eq (1), respectively:

$$\bar{U} = \frac{1}{N}\sum_{i=1}^{N} U_i \tag{1}$$

Where U_i is the instantaneous wind velocity magnitude at the i time step, N is the total number of time step. For the wind turbine power output is calculated using the Eq (2):

$$P = M \cdot n \cdot \frac{2\pi}{60} \tag{2}$$

Where M is the sum of the torque generated by the three blades, n is the rotational speed of wind turbine.

The turbulence model selected for this paper is the SST k-ω model. Reference [33][34] has confirmed that the SST k-ω model has high accuracy in wind turbine simulation results. The k is the turbulent kinetic energy. Thus, the k data can be obtained directly from the CFD simulation. The sampling of TI and k values is similar to the wake velocity, and the average TI is calculated using Eq. (3).

$$TI = \frac{\sqrt{6k}}{3U_{hub}} \tag{3}$$

Where U_{hub} is the wind velocity at hub height.

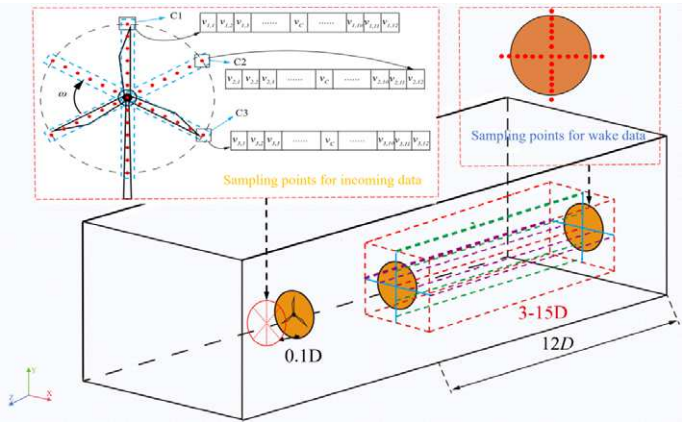

Fig. 3. Sampling point arrangements for incoming and wake data

2.3 Elliptical fitting method for wake velocity distribution

This paper fits the asymmetric wake velocity distribution using an elliptical 3D Gaussian model at a cylindrical coordinate system. Velocity data are obtained from four azimuthal monitoring points (u_{p+}, u_{p-}, u_{v+}, u_{v-}). The azimuths of these four monitoring points differ by 90°at each radial location to construct elliptical velocity distribution shown in Fig. 4. And their velocity values are exactly the long and short axes of the elliptical velocity profile. Since the velocity distribution is asymmetric at the vertical slice which is perpendicular to z axis, four elliptical velocity distribution at four quadrants are gained separately and form a whole wake velocity distribution. Eq (4) is the description of this elliptical fitting method which takes u_p and u_v as input.

$$u(r,\boldsymbol{\theta},z)=u_p(r,z)u_v(r,z)\Big/\sqrt{u_v^{\,2}(r,z)\cos^2\boldsymbol{\theta}+u_p^{\,2}(r,z)\sin^2\boldsymbol{\theta}} \tag{4}$$

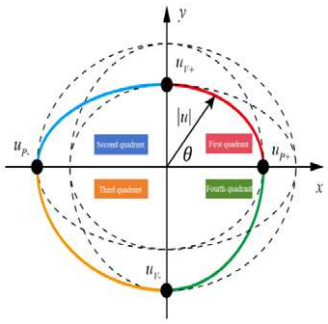

Fig. 4. Schematic of radial annular wake fitting

2.4 Wind farm prediction methods based on CNN and GAN

As shown in Fig. 5, the wind farm prediction system method proposed in this paper consists of four principal modules, which are the G_{in}, the G_{w}, the R, and the P. The G_{in} is used to generate the high-dimensional incoming speed distribution of the wind turbine using the incoming flow conditions (V_{in} and TI). The high-dimensional incoming speed distribution is then inputted to P module, R module and G_{w} module to predict the power, rotational speed the wake distribution of wind turbine. The incoming condition of the downstream wind turbine can be gained from the wake distribution of upstream wind turbine when the location of the downstream turbine is determined in the wake region. This process is repeated until the power output and rotational speed values of the last turbine in the wind farm are calculated.

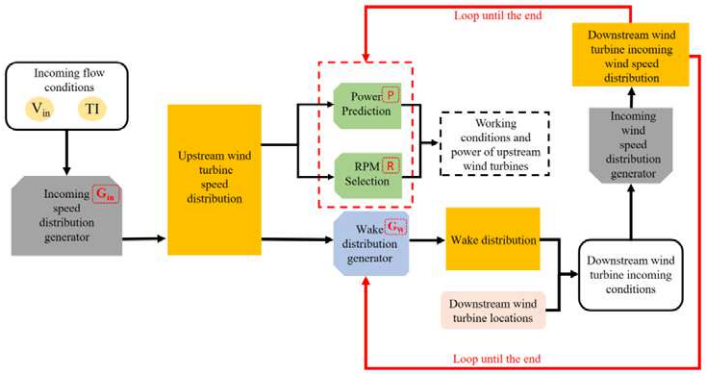

Fig. 5. Wind farm prediction system method

2.4.1 Incoming speed distribution generator module and model training framework

The G_{in} is developed to gain high-dimensional incoming data. This module is primarily constructed using a transposed convolution method. It consists of four network layers using the V_{in} and TI as input. The fully connected layer expands it into five neurons. Subsequently, the transposed convolution layer is employed to construct the feature map, and the batch normalization layer (BN) is used to normalize feature map. The convolution layer is used to reproduce the flow field features. The kernel size, padding, stride and receptive field are illustrated in Fig. 6 for of the convolution layer.

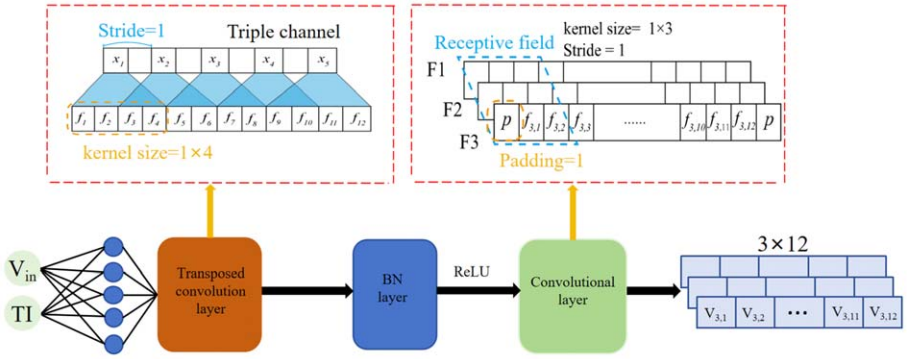

Fig. 6. G_{in} structure

The CGAN structure is suitable for the surrogate modeling of parametrized fluid flows, as the unique correspondence between the flow parameter and the flow field can be established [29]. Therefore, the G_{in} is trained using the CGAN structure to establish a mapping between the incoming flow conditions and the high-dimensional incoming data. The CGAN structure is shown in Fig. 7. Speed distribution module (D_{in}) is used as a discriminator and G_{in} is used as a generator. In addition, the matchmaker network (G_{in}^{-1}) is added to the model for joint

objective training, and the role of G_{in}^{-1} is to generate the predicted incoming conditions which are compared to the real incoming conditions. The incoming flow conditions are input to the G_{in} to generate predicted high-dimensional incoming data. The predicted high-dimensional incoming data and the real incoming flow conditions are input to the D_{in} to determine true and false data. Meanwhile, G_{in}^{-1} reproduce the predicted incoming data generated by the G_{in} to the prediction incoming flow conditions. The prediction incoming flow conditions are compared with real incoming flow conditions to determine true and false data. The errors of both D_{in} and G_{in}^{-1} are used to train the G_{in}. The G_{in} training, the D_{in} training and G_{in}^{-1} training are carried out alternatively until the D_{in} can produce realistic flow data that is not distinguishable from the real flow data obtained by the high-fidelity simulations.

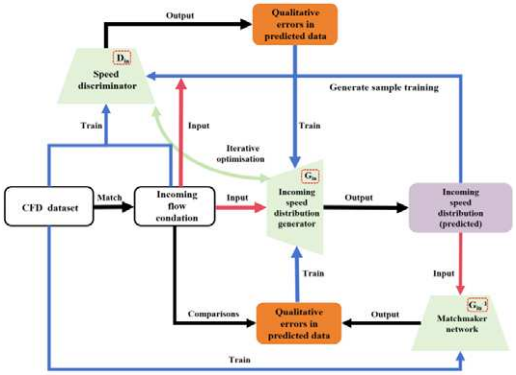

Fig. 7. CGAN training system

The structure of the D_{in} and G_{in}^{-1} in the CGAN model is shown in Fig. 8. The D_{in} structure inputs the incoming speed distribution to the CNN-B network to obtain eight outputs. The incoming flow conditions are combined with the eight outputs into a fully connected layer, and the final output is J which respects true and false data . The G_{in}^{-1} structure inputs the incoming speed distribution and outputs incoming flow conditions. The G_{in}^{-1} structure is an inverse derivation model, so it is suitable for direct backpropagation (BP) training. The model is pre-trained separately before the GAN network undergoes learning.

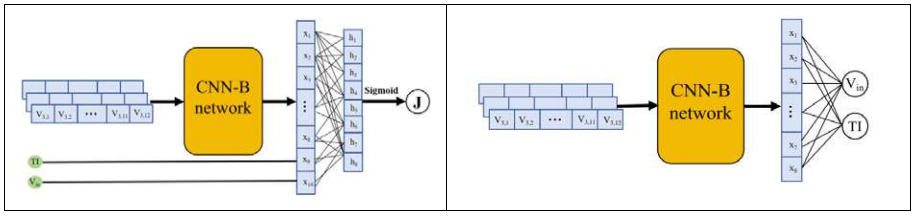

(a) Structure of D_{in}	(b) Structure of G_{in}^{-1}

Fig. 8. Structure of D_{in} and G_{in}^{-1}

To better evaluate the training results of the G_{in}, this paper introduces a criterion: the average absolute error function ($L1\_loss$) to monitor the accuracy of the model. As shown in equation (5), the error function is defined as the average of the absolute value of the difference between a set of predicted value and the corresponding true value.

$$L1\_loss = \frac{1}{N}\sum_{i=1}^{n}\left|x_i - x_i'\right| \tag{5}$$

where N is the sample number, x_i is the predicted value, x_i' is the simulation data.

2.4.2 The wake distribution generator model and model training framework

The Fig. 9 shows the wake prediction sub-model G_w network architecture. It integrates 13 wake velocity sub-networks (3D-15D) and a central point velocity network. Sub-3D network represents the wake velocity distribution at the position 3D downstream of wind turbine. Sub-3D network resolves velocity distributions at 32 monitoring nodes within two crossed lines excluding the central point. The advantage of this axial view is that it avoids the loss of model accuracy caused by axial segmentation along the z-axis as described in the reference[35].The central point velocity network is derived independently by a CNN-B module, which processes upstream flow field features and TI, and then generates axial velocity vectors via two fully connected hidden layers. The prediction of the center velocity is used to determine the V_{in} of the wind turbine at different distances (3D-15D) downstream. Combining TI values to obtain the downstream turbine front 0.1D incoming speed distribution.

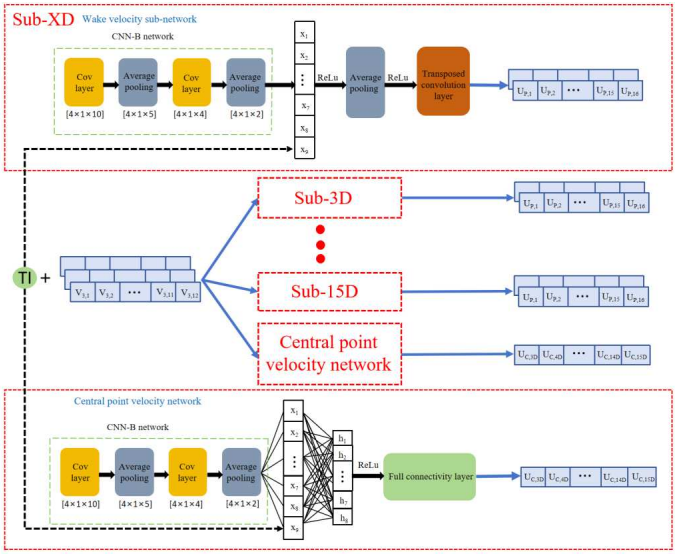

Fig. 9. Prediction network for wake region

This paper proposes a Cycle GAN architecture for training G_{w} network based on basic GAN. As illustrated in Fig. 10, Cycle GAN [36] training system employs four networks, namely the wake generative network(G_{w}), wake discriminator network (D_{w}), the wake matchmaker network(G_{wi}) and matchmaker discriminator network ($D_{\mathrm{in\_c}}$). The incoming speed distribution is derived from CFD simulation data and the G_{in} . The incoming speed distribution is inputted to the G_{w} for training purposes. The training target is the velocity data on the axial cross-section at a specified distance (3D-15D). The prediction of wake distribution generated by the G_{w} are input to the D_{w} network to compute the G loss and D loss. The predicted wake data are also input the G_{wi} to reproduce the incoming speed distribution. This process completes a data reproduce. The G_{wi} training and $D_{\mathrm{in\_c}}$ training are carried out alternatively until the G_{wi} can produce realistic incoming speed distribution that is not distinguishable from the real flow data obtained by the high-fidelity simulations. Finally, the predicted incoming speed distribution are mapped back to the wake distribution through G_{w} .

The $L1\_loss$ result is calculated as the loss between the wake distribution obtained through reproducing the wake distribution and the wake distribution generated by the G_{w} .The loss function of the G_{w} in Cycle GAN is the joint loss of the G_{w}_loss and the $loss1$ (compare predicted incoming speed distribution with training incoming speed distribution). The loss function of the G_{wi} is the joint loss of the G^{-1}_loss and the $loss2$ (compare predicted wake distribution with reproduced wake distribution). Each epoch will train the G_{w} , D_{w} , G_{wi} , and $D_{\mathrm{in\_c}}$ simultaneously.

The G_{w} joint loss function and G_{wi} joint loss function formulas are shown below:

$$Loss\left(G_{W}\right)=\frac{1}{2}\left[G_{W}\_loss_{(BCE)}+loss1_{(MSE)}\right] \tag{6}$$

$$Loss\left(G_{Wi}\right)=\frac{1}{2}\left[G^{-1}\_loss_{(BCE)}+loss2_{(MSE)}\right] \tag{7}$$

Where G_{W}_loss and G^{-1}_loss are generation losses, $loss1$ and $loss2$ are cyclic consistency losses.

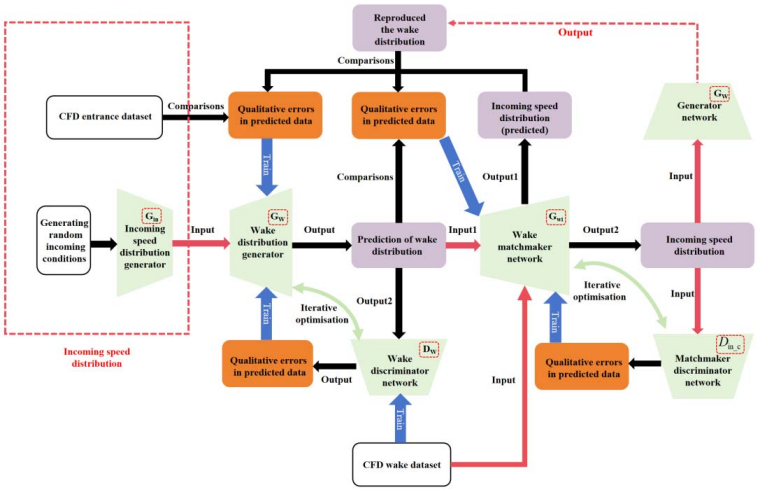

Fig. 10. Cycle GAN training system

2.4.3 The rotational speed prediction module

Rotational speed selection is critical to prevent blade flow separation and maximize power output, as excessive speeds induce flow separation that reduces energy capture. Rotational speed must dynamically match to incoming speeds, particularly in large-scale wind farms where spatial wind speed variations necessitate turbine-specific adjustments. Therefore, a R model is established [37]. As shown in Fig. 11, the R model consist of a CNN-B module as the primary component, with a hidden layer consisting of seven nodes corresponding to the seven speeds listed in Table 2.

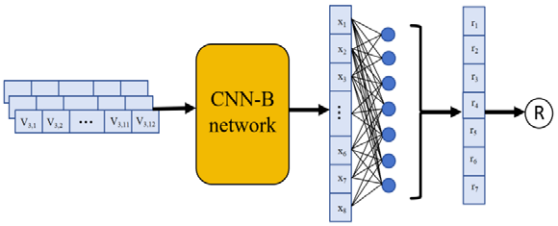

Fig. 11. Structure of rotational speed prediction module

2.4.4 The power prediction module

The inputs to the P module are the high-dimensional incoming data and TI, and the output is the power of the wind turbine. As shown in Fig. 12 (a), the incoming speed distribution are input to the CNN-B network and after deriving the 8 feature outputs of the CNN-B, the TI inputs are added to mix with it. After inputting the mixed result

into a fully connected layer (8 neurons), the predicted power result is again calculated fully connected through the nonlinear activation process of ReLU. To obtain TI data in the downstream region, it is necessary to construct a network for predicting TI. As shown in Fig. 12 (b), the input parameters of the TI prediction model are the incoming speed distribution and TI at different downstream distances, and the output is the TI in 3D-15D.

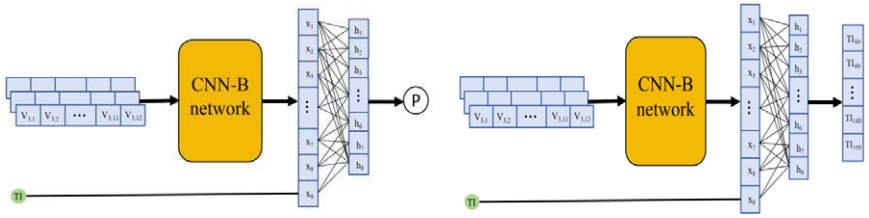

(a) P model structure (b) TI prediction model

Fig. 12. P and TI structure

3. Results and discussion

In section 3, the performance of the proposed wind farm prediction system is evaluated and discussed. Section 3.1 validates the accuracy of our CFD simulation data compared with that of experiments or LES. The training and validation of the power and rotational speed model are described in Section 3.2. Section 3.3 evaluates the training results and validation of the incoming speed distribution generation model based on CGAN. The prediction performance of the wake distribution generation model of the proposed Cycle GAN is evaluated in Section 3.4. In Section 3.5, the calculation results of two wind turbines are compared with the model prediction results, and a velocity correction for the downstream wind turbine is proposed, which makes the prediction results closer to the simulation results. In Section 3.6, Power prediction for multiple wind turbines is performed using real wind farm data validation to verify the use in wind farm applications.

To further quantify prediction accuracy and the accuracy of the simulation results, the mean percentage error (MAPE) and the coefficient of determination (R^2) are calculated to evaluate the model performance on testing datasets. The MAPE is defined as follows.

$$MAPE = \frac{100\%}{N}\sum_{i=1}^{n}\left|\frac{x_i - x_i'}{x_i'}\right| \tag{8}$$

where N is the sample number, x_i is the value or simulation data, x_i' is the predicted data.

R^2 is a statistical measurement that reflects the fit quality of a regression model. It evaluates the model capacity

to explain variability in the data. The equation of R^2 is expressed as follows[38]:

$$R^2 = 1 - \frac{\sum_{i-1}^{n}(Y_i - \hat{Y}_i)^2}{\sum_{i-1}^{n}(Y_i - \overline{Y})^2} \tag{9}$$

where n is the sample number, Y_i is the i^{th} actual value, $\hat{Y}_i$ is the i^{th} predicted value, and $\overline{Y}$ is the average of true value.

3.1 Verification the data gained from the full-model CFD simulation

It is critical importance to validate the reliability in simulating wind turbine output power, wake characteristics. To ensure the convergence and reliability of the full-model CFD data, this paper conducts simulation validation of the full-model wind turbine under the conditions of different wind speeds and rotational speeds. The power data are verified by comparing them with the actual data from the reference [31]. As shown in Fig. 13, the value of MAPE is 3.17% in the wind speed range of 5 m/s to 11.4 m/s, the simulated power results align with the overall trend.

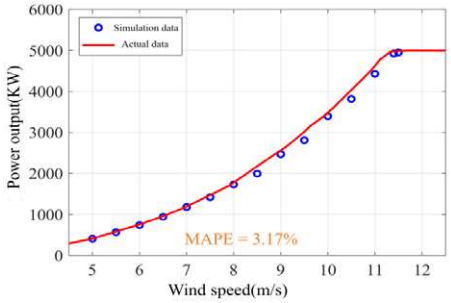

Fig. 13. Verification of wind turbine power output

The velocity distributions obtained from the full-model simulation were compared with high-precision LES and experimental date [39][40] for validation, as shown in Fig. 13.The 3D-15D wake flow field downstream of the wind turbine was monitored at rated wind speed and rotational speed. For vertical cross-section distribution in the near wake region, the MAPE values is 8.36% and 9.13% for the 3D and 6D, respectively. The wakes velocity is larger near the center, and the wake velocity is smaller on both sides of the rotor blade tip. This simulation result is in accordance with the data gained by the LES. As the flow develops, the downstream high velocity and low velocity wake mix, the "W" shape distribution is transfer to smooth velocity distribution. In the far wake (10D), the wake distribution is the smooth velocity distribution due to the full development of the flow field. The MAPE values is 6.26% smaller than the near wake region. For horizontal cross-section distribution, the MAPE values is 8.28% and 6.17% for the 3D and 5D, respectively. As the flow develops, the downstream high velocity and low velocity wake mix, the "W" shape distribution is transfer to "U" shape distribution. For average central point velocity of the wind

turbine, the MAPE value is 2.54%. It can be observed that as the flow develops, the central velocity begins to recover gradually A comprehensive comparison indicates that the simulated velocity distribution in this paper is reliable and has reference value.

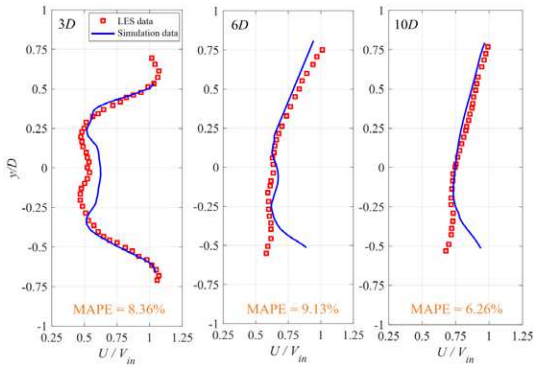

(a) Vertical cross-section velocity distribution along x direction

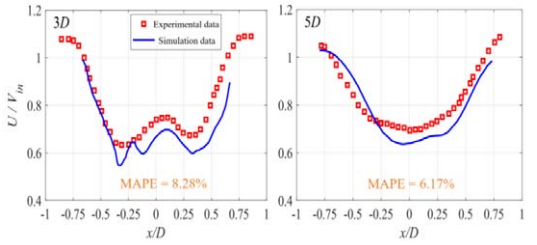

(b) Hub height radial velocity distribution along y direction

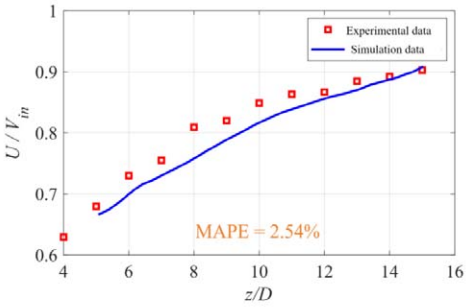

(c) Average central point velocity of the wind turbine

Fig. 14. Validation of simulated flow field

3.2 Validation of the power and rotational speed prediction models

Fig. 15 shows the number of occurrences of different R level. The actual R level of 2, 4, 6, and 7 are misjudged at a higher level of RPM. It can be analyzed that all the misclassified data are generated by the V_{in} near the RPM shift junction in Table 2. This prediction error may be caused by insufficiently dense data in the RPM transform junction. The interval between these V_{in} needs to be minimized to avoid model impact.

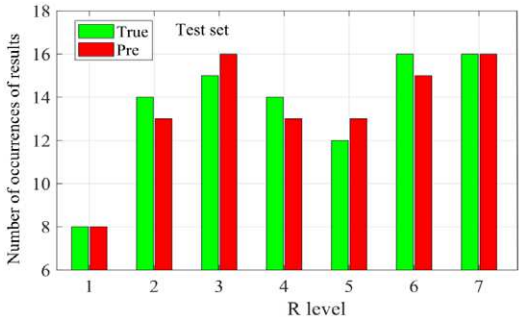

Fig. 15. Number of occurrences of different R level predictions

For the training and validation of the P model is shown in Fig. 16. The overall model prediction data fit the actual data better, and the statistical index R^2 of the prediction data in both the training and test sets exceeds 0.99, which indicates that the model fits the CFD monitoring data well and has good prediction accuracy.

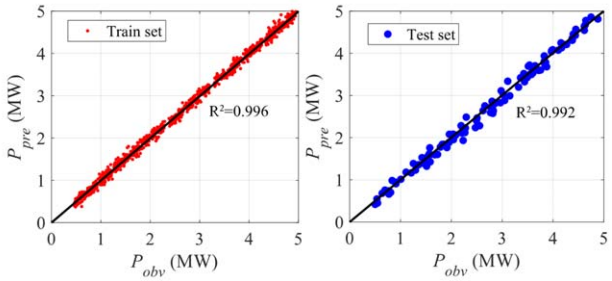

Fig. 16. Scatter plot of P model prediction distribution

3.3 Validation of incoming speed distribution generator model based CGAN

The changing values of the loss function during the training process of the G_{in} network is shown in Fig. 17. The change of G_loss and D_loss function is negatively correlated, showing the trend of this and the other. Observing the trend of $L1\_loss$, the D_{in} network at the beginning stage has a higher discrimination rate for the

crude data generated by the G_{in} network, which leads to a more difficult training of the G_{in} network at the beginning. After more than 500 Epochs, the G loss is smaller than the D loss, currently, and the $L1\_loss$ begins to decline steadily, and stops after learning 4000 Epochs for the training set, and the trained parameters are selected to construct the G_{in}.

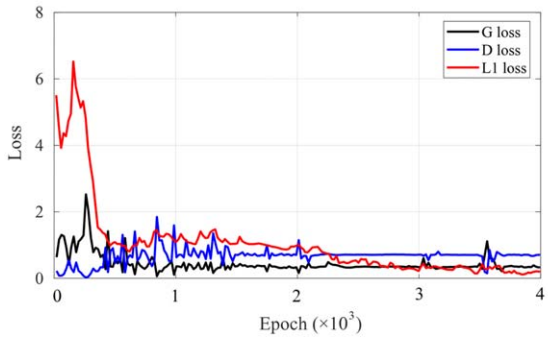

Fig. 17. CGAN training process

Fig. 18 shows the errors for each data point in the prediction results of the G_{in} for the test set. The results show that the distribution of prediction errors for the points on all three lines C1, C2, C3 are around 3%. This results confirm the modeling accuracy of the G_{in}.

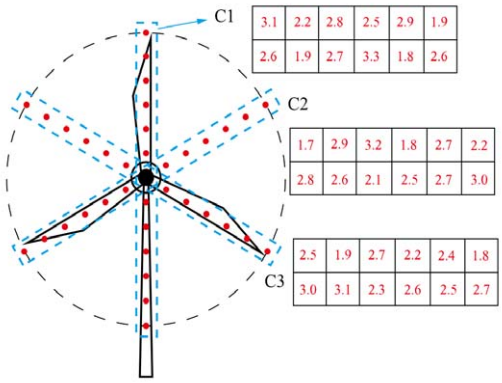

Fig. 18. Incoming speed error

3.4 Adversarial training of Cycle GAN-Based wake generation models with validation

3.4.1 Cycle GAN network training

A Cycle GAN structure comprises six loss functions, which are used to train the four networks simultaneously.

Among these $loss$ functions, the $L1\_loss$ result of G_w is of important indicators, as it reflects the degree of matching between the wake flow and its corresponding incoming flow. The training process for each Sub-network within the Cycle GAN structure is illustrated in Fig. 19. The performance of the cross-section velocity Sub-networks (3D-15D) varies in response to the training cycle. It can be observed that the loss function of the Sub-3D in the near wake flow region exhibits greater fluctuations, while the training efficiency of the sub-network model in the far wake flow region improves with increasing distance. After 3000 epochs, there has been no significant decline in the $L1\_loss$ value, thus the sub-network model parameters have largely stabilized. At this moment, the model parameters are chosen to predict the velocity of the wake field.

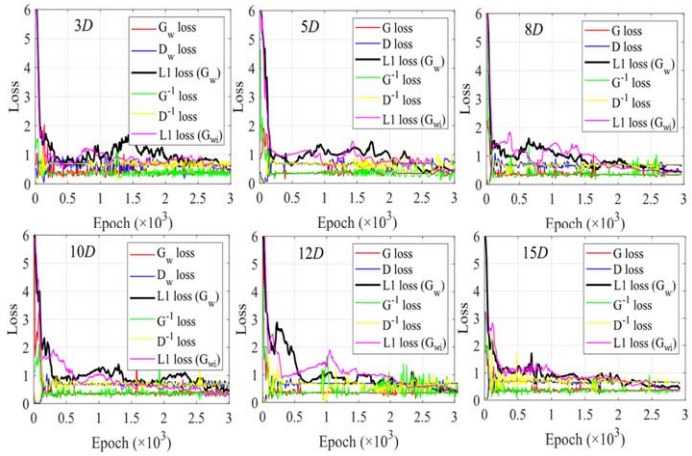

Fig. 19. Cycle GAN training process

3.4.2 Verification of wake prediction data

Fig. 20 present a comparison between the predicted values and CFD simulation data of the wake velocity distribution at different distance along z-axis. The MAPE values are all below 9%. Fig. 19 (a) illustrates the wake velocity distribution in the y direction (3D to 8D), Fig. 20 (b) shows the wake velocity distribution in the x direction (3D to 10D). From Fig. 20 (a), it is evident that the predicted data do not align well with the CFD data in the range of -0.5<X/D<0.5, and the disparity is especially occurring in the range of -0.5<X/D<0, at the 3D downstream of wind turbine. The lower linear velocity in the blade root region leads to underutilization of the incoming flow energy passing through the wind turbine center area. A higher residual kinetic energy remains in the near wake, causing a relatively large velocity loss in the central wake region. In the near wake region, the low velocity wake on both sides does not sufficiently mix with the high velocity airflow in the wind turbine center area, resulting in "W" shape of velocity profile. The wake generation sub model has a lower accuracy prediction of this "W" shape of velocity profile. When downstream distance is larger than 3D, the velocity profile is "U" shape due to the mixing of the high and low speed airflow. The wake generation sub model has a higher accuracy prediction of this "U" shape of velocity profile. The variation of velocity along the x and y direction may has a certain impact on the prediction accuracy of

wake generation sub model. However, since downstream wind turbines are usually located in the far wake region of upstream wind turbines in the wind farm layout, the near wake prediction accuracy has less impact on the optimization of wind turbine layout.

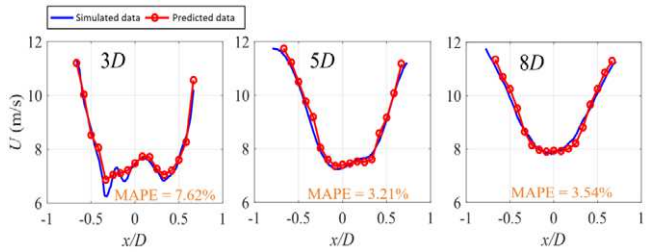

(a) Hub height radial velocity distribution along y direction

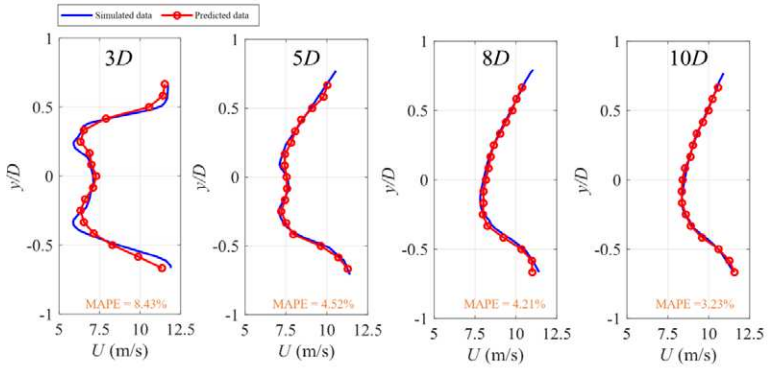

(b) Vertical cross-section velocity distribution along x direction

Fig. 20. Comparison of wake prediction results

Fig. 21. Predicted velocity distribution compares the prediction results of the Jensen-Gaussian analytical wake model [14], the ANN wake model and the CNN-GAN wake model. The ANN wake model is a line wake network trained by BP, and the CNN-GAN wake model is an axis section network model trained by Cycle GAN. For the 3D downstream of the wind turbine, the CNN-GAN wake model obtained a MAPE of 3% for the velocity prediction data versus the full model CFD simulation data at each point. the ANN wake model had a MAPE of 3.7% versus the full model CFD simulation data. This shows that the prediction accuracy of the ANN wake model is low compared to the CNN-GAN wake model. The Jensen-Gaussian model is not accurate enough compared to CNN-GAN wake model and ANN wake model. This is attributable to the assumption of a steady-state Gaussian distribution, whilst vortex interactions are ignored. It leads to oversimplification in 3D. For the 10D downstream region of the wind turbine, the CNN-GAN wake model obtained a MAPE of 1.5% in the comparison of the velocity prediction data with the CFD simulation data at each point. In contrast, the ANN wake model had a MAPE of 3.4% in the comparison of the CFD simulation data. This is due to the fact that the advantage of the axial part of the GAN

network in continuous deconvolution makes the predicted data closer to the CFD simulation data. The BP linear network has the capacity to generate radial velocity gradients that are non-existent, thereby resulting in a lower level of prediction accuracy when compared to the CNN-GAN wake model. In the GAN structure, the discriminator network effectively avoids this problem. In real wind farms, downstream wind turbines are usually located in the far wake zone of upstream wind turbines, so the accuracy of data in the far wake zone is even more important. In summary, the CNN-GAN wake model has better prediction performance than the ANN wake model in the far wake region.

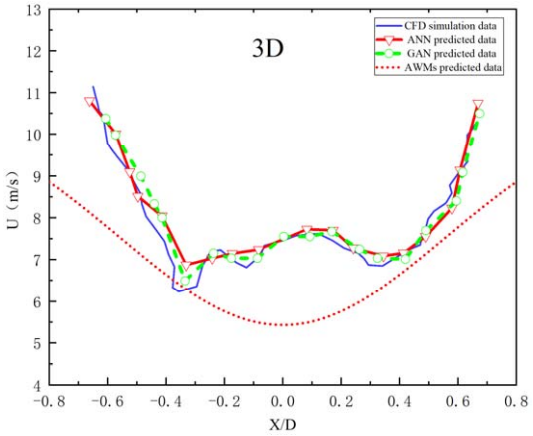

(a) Predicted velocity distribution at 3D

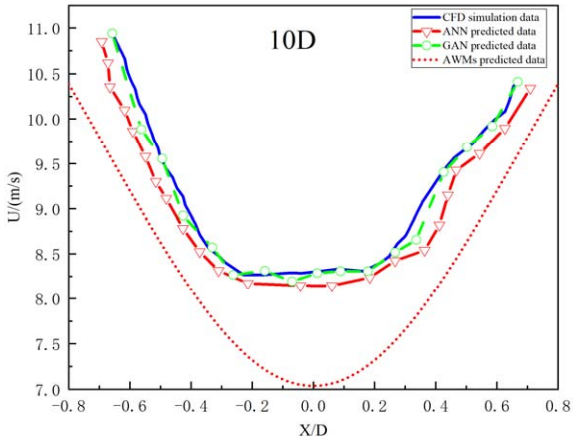

(b) Predicted velocity distribution at 10D

Fig. 21. Predicted velocity distribution

The velocity data (u_{p+}, u_{p-}, u_{v+}, u_{v-}) at each radial position are substituted into Eq. (4) and fitted to obtain a continuous distribution of velocities in the radial annulus (along z-axis). Fig. 22 shows the wake velocity distributions at different axial distances (3D-8D) and radial positions (0.25D-0.5D) under different V_{in}. It is observed that there is a similarity in the velocity distributions of the wake flow, with low V_{in} corresponding to lower wake velocities. However, the characteristics of the wake velocity distributions do not change much when V_{in} is different. The velocity profile in the near wake region is relatively irregular, and the distribution derived from Eq. (4) simplifies some of the flow details in the near wake region. However ,the velocity distribution in the radial annulus is more regular after 5D, and the fitted predicted velocities are more in line with the original velocities distribution.

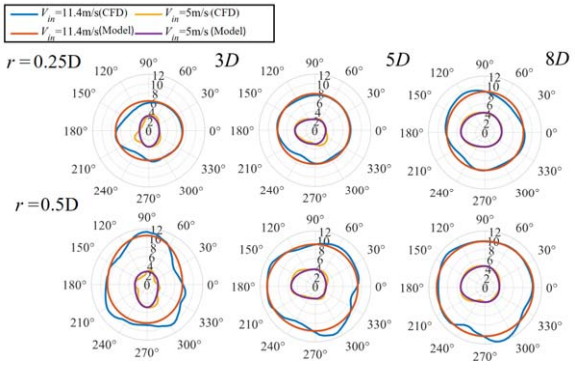

Fig. 22. Results of wake model fitting

3.5 Verification and correction of tandem wind turbine wake prediction

To verify the prediction performance of the wake prediction model in tandem arrangement, the data obtained from CFD simulations and model predictions are compared in Fig. 23 (a) shows that the output power prediction results. The red bars represent the upstream wind turbine output power, while the blue bars indicate the downstream wind turbine output power result. The data in red color indicates the power value of the upstream wind turbine and the data in blue color indicates the output power result of the downstream wind turbine. It found that the predicted output power of the upstream wind turbine is 4.69% higher than the CFD data, while the predicted output power of downstream wind turbine is 6.07% higher than the CFD data. The reason for this error may be the large upstream TI prediction, which leads to the large power prediction of the downstream wind turbine. Fig. 23 (b) shows the predicted results of the TI and central point velocity for different axial distances (3D-14D). The red line represents the model predicted data of the central point velocity, the black line represents the CFD data of the central point velocity, the green dots represent the model predicted TI at different distances, and the blue dots represent the TI

obtained from the CFD simulations. For TI, the predicted results are slightly higher than the CFD results in the upstream region and slightly lower than the CFD results in the downstream region. For the central point velocity, it can be observed that the central velocity recovery rate of the downstream wind turbine (11D-14D) is significantly larger than the model prediction. This prediction error of the downstream central point velocity is mainly because that the decrease in the prediction of upstream central point velocity, which leads to a decrease in the downstream central point velocity.

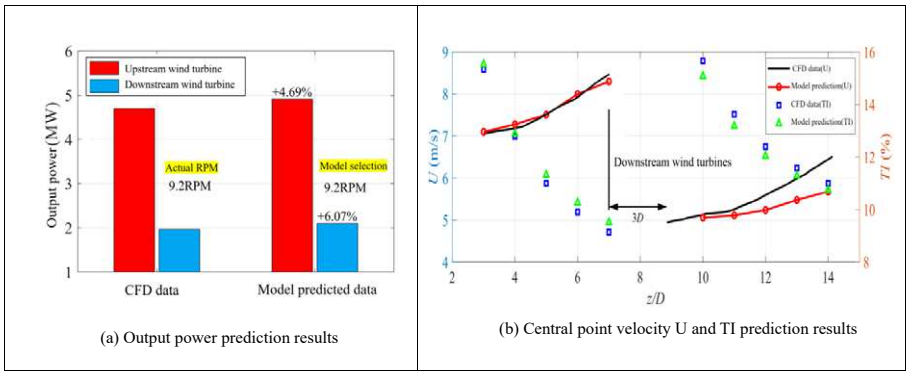

(a) Output power prediction results

(b) Central point velocity U and TI prediction results

Fig. 23. Tandem twin wind turbine prediction results

The G_w network is constructed by the data of a single wind turbine, which does not consider the mixing effect of the mixing of high velocity flow and low velocity wake on the wake velocity recovery of the downstream wind turbine. The high velocity flow adds more momentum to the far wake region of the downstream wind turbine, resulting in faster wake recovery in the far wake region. Therefore, the momentum supplement is proposed to correct the wake velocity at the far wake region of the downstream wind turbine and the specific methods are as follows. After the incoming flow conditions of downstream wind turbine were inferred from the G_w , G_{in} and TI networks, the model inputs for the downstream wind turbine Sub-5D and beyond were actively adjusted. The final V_{in} inputs for these sub-networks were taken to be the average of the actual predicted results and the V_{in} of upstream wind turbine.

The corrected wake distribution prediction along y direction is shown in Fig. 24 . The black line represents the downstream wind turbine CFD data, the red line represents the radial velocity distribution in the y-direction obtained when the correction V_{in} is not applied with the momentum addition method, and the blue line represents the radial velocity distribution in the y-direction obtained when the correction V_{in} is applied with the momentum addition method. The predicted velocity before correction is significantly smaller than the CFD calculation results. By correcting the V_{in}, it is evident that at downstream distances of 5D and 7D, the improved prediction results can match well with the simulation results.

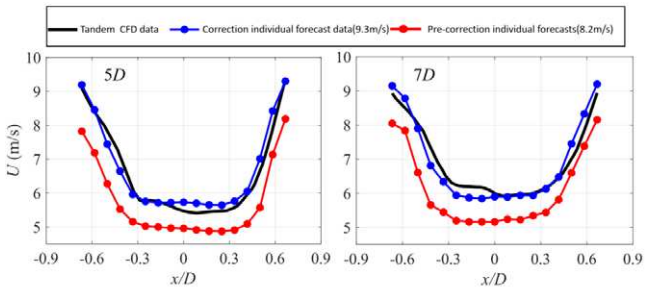

Fig. 24. Downstream velocity correction

3.6 Power prediction for multiple wind turbines

To examine the performance of the proposed system in wind farm applications, the power prediction of multiple wind turbines is conducted for the Horns Rev 1 wind farm [41] for real wind field data verification. The overall layout of the wind turbines is in the form of a parallelogram. The overall layout of the wind turbine array is in the form of a parallelogram, with a total of 8 groups in the east-west direction, 10 rows of wind turbines in each group, and upstream and downstream wind turbines spaced at 7 D. The validation inputs to the wind farm prediction system in this section will be consistent with the incoming wind conditions from the measured data, choosing three incoming wind directions 270° , 220° and 312°, with the ambient wind speed set to 8 m/s and TI = 7.7%.

Since the wind turbine specifications in the Horns Rev 1 wind farm are different from the 5MW wind turbine used for training in this paper, the data needs to be standardized in a uniform way before proceeding to the next step of prediction. In this paper, the power curves of the wind turbines are taken as objects to be standardized, and the formulas are shown in Eq. 8. The standardized power curves of the two processed wind turbines are presented in Fig. 25. It can be observed that the two curves exhibit a high degree of fitting, and that the thrust coefficients of the two wind turbines are similar under the standardized operating conditions.

$$f_{P,1}\left(\frac{V_{in,1}-V_{\min,1}}{V_{rate,1}-V_{\min,1}}\right)\Big/ P_{rate,1} \approx f_{P,2}\left(\frac{V_{in,1}-V_{\min,2}}{V_{rate,2}-V_{\min,1}}\right)\Big/ P_{rate,2} \tag{8}$$

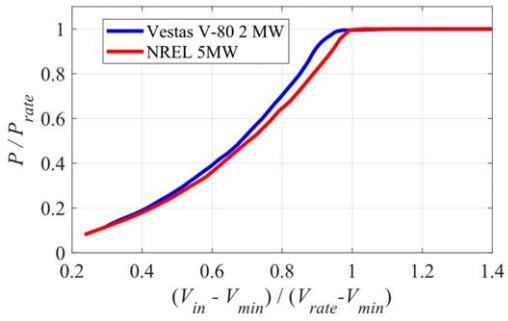

Fig. 25. Standardized power curve

Fig. 26 presents the normalized power output of the wind farm array under three distinct wind directions, comparing the prediction system developed in this paper against both field measurements from the Horns Rev offshore wind farm [42] and LES results [41]-[43]. The red line represents predicted data, the blue line represents LES data, and the black line represents actual measurement data. From the results, the wake effect of the first wind turbine causes a 30–40 % power generation loss for the second wind turbines. The power at the third wind turbine is slightly reduced compared to the second wind turbine because of the variation by the TI affecting the wake recovery rate. Starting from the second wind turbine, the combination of superimposed wake and accelerated wake recovery results in dynamic equilibrium conditions, which allow subsequent wind turbines to have the same level of power output.

For the predicted power in the 270° wind direction, the red dashed line represents power results predicted by the uncorrected model. The third wind turbine of the uncorrected model has decreased to a level below 30% of the power prediction of the first wind turbine. The subsequent wake speed is already below the wind turbine's cut-in speed, which renders the downstream wind turbine unable to operate normally. For the power prediction results of the modified model, it can be seen that the power gradually stabilizes from the third wind turbine onwards, and the prediction results are close to the LES prediction. The stabilization of the trend in this wind direction may be due to the symmetrical layout of the wind turbines. It can be seen that by adjusting the downstream V_{in}, the problem of excessive velocity decay in the far wake region predicted by the model and accurately predict the wind turbine power.

For the predicted power in wind directions of 222° and 312°, the results for the first two turbines match the actual measurement data. However, the results for the third turbine onwards are progressively lower than the actual measurement data, although the overall trend remains consistent. This prediction error can occur due to lateral shifts in the wake diffusion path in inclined wind direction. Comparing LES data with the predicted data in 312° wind direction, the power simulation results for the second wind turbine LES are significantly smaller. The downstream power of such a tandem wind turbine is less than the power results of the downstream turbine for full-model CFD simulation[44][45], which can also be observed in LES and actuator studies [46]-[48]. This may be due to the error caused by the simplification of the ALM.

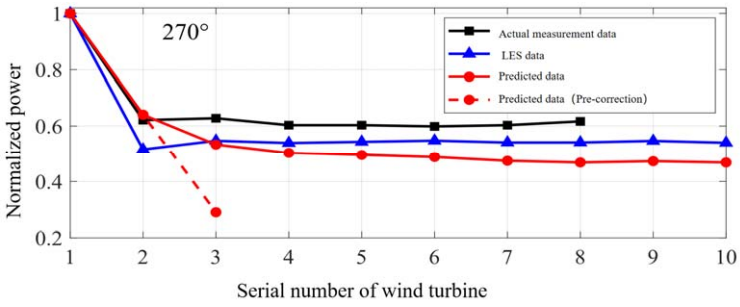

(a) 270°

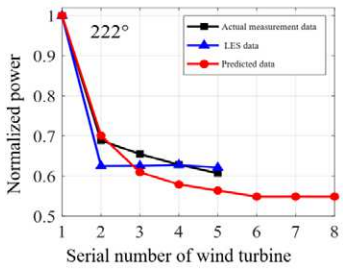

(b) 222°

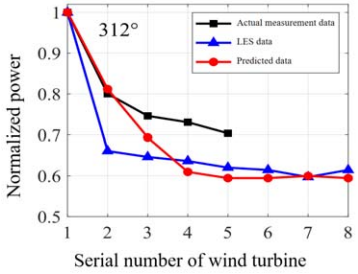

(c) 312°

Fig. 26. Comparison of predicted power of real wind farms

4 Conclusion

To ensure the accuracy and efficiency for predicting wind turbine wake and output power, a surrogate modeling system using full-model CFD and CNN-GAN was developed in this study to establish a power prediction system for wind farms comprising multiple wind turbines. The system uses CNN models to construct prediction models for the NREL 5 MW wind turbine under different incoming conditions. The CNN models are trained using the data from a full-model CFD and the GAN frameworks. The prediction performance of the proposed model is evaluated comprehensively and following conclusions are obtained.

(1) The innovative design of the CGAN-based incoming speed distribution generator can obtain the high-dimensional incoming speed at the 0.1D position in front of the turbine, just by inputting the V_{in} and TI. The model solves the problem of difficulty in obtaining the flow field data in front of wind turbine. The generation speed is greatly improved compared with the traditional CFD simulation, and the error is controlled within 3%. The design

of the G_{in} greatly enhances the engineering applicability of the prediction system.

(2) The wake prediction model is divided into several velocity distribution sub-networks with axial cross sections, and a function is fitted to the discrete data to form a 3D wake model. To address the problem of matching the wake velocity distribution with the incoming speed distribution at each cross section, a reflective projective model is developed for dual objective joint training using a cycle GAN structure. The results show that the GAN-trained model produces results that are consistent with the actual physical scenario and are highly accurate in the far wake region.

(3) The downstream wind turbine center speed is corrected according to the principle of momentum complementation, and the corrected system is applied to the total power prediction of wind farms. The computational results show that the power prediction of LES is basically consistent with the results calculated by the model, indicating that the model has good performance in wind farm power calculation. The validation shows that the wind farm prediction system can greatly improve the prediction speed while ensuring the prediction accuracy, which is of great value for engineering applications.

Future work may involve the study of wake prediction for wind farms in complex terrain on hillsides. Another direction is to explore the use of the developed model for optimal control design in wind farms.

Acknowledgment

The authors express their great thanks to National Key R&D Program of China. Project Number: 2024YFA1012501 for financial support.

Data availability

The data that support the findings of this study are available from the corresponding author upon reasonable request.

Reference

[1] Bai C J, Wang W C. Review of computational and experimental approaches to analysis of aerodynamic performance in horizontal-axis wind turbines (HAWTs). Renewable and Sustainable Energy Reviews, 2016, 63: 506-519. https://doi.org/10.1016/j.rser.2016.05.078

[2] Yu Z, Zheng X, Ma Q. Study on actuator line modeling of two NREL 5-MW wind turbine wakes. Applied Sciences, 2018, 8(3): 434. https://doi.org/10.3390/app8030434

[3] Songyue L I U, Qiusheng L I, Bin L U, et al. Prediction of offshore wind turbine wake and output power using large eddy simulation and convolutional neural network. Energy Conversion and Management, 2025, 324: 119326. https://doi.org/10.1016/j.enconman.2024.119326

[4] Mo J O, Choudhry A, Arjomandi M, et al. Effects of wind speed changes on wake instability of a wind turbine in a virtual wind tunnel using large eddy simulation. Journal of Wind Engineering and Industrial Aerodynamics, 2013, 117: 38-56. https://doi.org/10.1016/j.jweia.2013.03.007

[5] Hou G, Wang J, Fan Y. Wind power forecasting method of large-scale wind turbine clusters based on DBSCAN clustering and an enhanced hunter-prey optimization algorithm. Energy Conversion and Management, 2024, 307: 118341.

[6] JENSEN N O. A NOTE ON WIND GENERATOR INTERACTION . Roskilde, Denmark: Risø National Laboratory, 1983.

[7] FRANDSEN S, BARTHELMIE R, PRYOR S, et al. Analytical modelling of wind speed deficit in large offshore wind farms. Wind Energy, 2006, 9(1-2): 39-53. https://doi.org/10.1002/we.189

[8] GAO X, YANG H, LU L. Optimization of wind turbine layout position in a wind farm using a newly-developed two-dimensional wake model. Applied Energy, 2016, 174: 192-200. https://doi.org/10.1016/j.apenergy.2016.04.098

[9] TAO S, XU Q, FEIJóO A, et al. Nonuniform wind farm layout optimization: A state-of-the-art review. Energy, 2020, 209: 118339 https://doi.org/10.1016/j.energy.2020.118339

[10] SUN H, YANG H. Study on an innovative three-dimensional wind turbine wake model. Applied Energy, 2018, 226: 483-493. https://doi.org/10.1016/j.apenergy.2018.06.027

[11] HE R, YANG H, SUN H, et al. A novel three-dimensional wake model based on anisotropic Gaussian distribution for wind turbine wakes. Applied Energy, 2021, 296: 117059. https://doi.org/10.1016/j.apenergy.2021.117059

[12] LIANG X, FU S, CAI F, et al. Experimental investigation on wake characteristics of wind turbine and a new two-dimensional wake model. Renewable Energy, 2023, 203: 373-381. https://doi.org/10.1016/j.renene.2022.12.070

[13] LING Z, ZHAO Z, LIU Y, et al. A three-dimensional wake model for wind turbines based on a polynomial distribution of wake velocity. Ocean Engineering, 2023, 282: 115064.

[14] GAO X, LI B, WANG T, et al. Investigation and validation of 3D wake model for horizontal-axis wind turbines based on filed measurements. Applied Energy, 2020, 260: 114272. https://doi.org/10.1016/j.apenergy.2019.114272

[15] KHAN M A, JAVED A, SHAKIR S, et al. Optimization of a wind farm by coupled actuator disk and mesoscale models to mitigate neighboring wind farm wake interference from repowering perspective. Applied Energy, 2021, 298: 117229. https://doi.org/10.1016/j.apenergy.2021.117229

[16] LIU L, STEVENS R J A M. Enhanced wind-farm performance using windbreaks. Physical Review Fluids,

2021, 6(7): 074611. https://doi.org/10.1103/PhysRevFluids.6.074611

[17] ONEL H C, TUNCER I H. Investigation of wind turbine wakes and wake recovery in a tandem configuration using actuator line model with LES. Computers & Fluids, 2021, 220: 104872. https://doi.org/10.1016/j.compfluid.2021.104872

[18] WANG T, CAI C, WANG X, et al. Evolution mechanism of wind turbine wake structure in yawed condition by actuator line method and theoretical analysis. Energy Conversion and Management, 2023, 281: 116852. https://doi.org/10.1016/j.enconman.2023.116852

[19] STEVENS R J A M, MARTíNEZ-TOSSAS L A, MENEVEAU C. Comparison of wind farm large eddy simulations using actuator disk and actuator line models with wind tunnel experiments. Renewable Energy, 2018, 116: 470-478. https://doi.org/10.1016/j.renene.2017.08.072

[20] ZHOU Y, XIAO Q, LIU Y, et al. Exploring inflow wind condition on floating offshore wind turbine aerodynamic characterisation and platform motion prediction using blade resolved CFD simulation. Renewable Energy, 2022, 182: 1060-1079. https://doi.org/10.1016/j.renene.2021.11.010

[21] FU S, LI Z, ZHU W, et al. Study on aerodynamic performance and wake characteristics of a floating offshore wind turbine under pitch motion. Renewable Energy, 2023, 205: 317-325. https://doi.org/10.1016/j.renene.2023.01.040

[22] MIAO W, LI C, PAVESI G, et al. Investigation of wake characteristics of a yawed HAWT and its impacts on the inline downstream wind turbine using unsteady CFD. Journal of Wind Engineering and Industrial Aerodynamics, 2017, 168: 60-71. https://doi.org/10.1016/j.jweia.2017.05.002

[23] YE M, CHEN H-C, KOOP A. High-fidelity CFD simulations for the wake characteristics of the NTNU BT1 wind turbine. Energy, 2023, 265: 126285. https://doi.org/10.1016/j.energy.2022.126285

[24] Li R, Zhang J, Zhao X. Deep learning-based wind farm power prediction using Transformer network. In: European control conference (ECC). IEEE; 2022.p. 1018–23. 2022. https://doi.org/10.23919/ECC55457.2022.9838022

[25] Sun H, Qiu C, Lu L, Gao X, Chen J, Yang H. Wind turbine power modelling and optimization using artificial neural network with wind field experimental data. Applied Energy 2020;280. https://doi.org/10.1016/j. apenergy.2020.115880

[26] Zhang J, Zhao X. A novel dynamic wind farm wake model based on deep learning. Applied Energy 2020;277. https://doi.org/10.1016/j.apenergy.2020.115552

[27] Li H, Yang Q, Li T. Wind turbine wake prediction modelling based on transformer-mixed conditional generative adversarial network. Energy, 2024, 291: 130403. https://doi.org/10.1016/j.energy.2024.130403

[28] LeCun Y, Bottou L, Bengio Y, Haffner P. Gradient-based learning applied to document recognition. Proc IEEE 1998;86:2278–324. https://doi.org/10.1109/5.726791

[29] Zhang J, Zhao X. Wind farm wake modeling based on deep convolutional conditional generative adversarial network. Energy; 2021.https://doi.org/10.1016/j.energy.2021.121747

[30] LI S, ZHANG M, PIGGOTT M D. End-to-end wind turbine wake modelling with deep graph representation learning. Applied Energy, 2023, 339: 120928.https://doi.org/10.1016/j.apenergy.2023.120928

[31] JONKMAN J, BUTTERFIELD S, MUSIAL W, et al. Definition of a 5-MW Reference Wind Turbine for Offshore System Development. Golden, CO, United States: National Renewable Energy Laboratory (NREL), 2009.https://doi.org/10.2172/947422

[32] Yang H, Chen J, Zhang Y, et al. Analysis of wake recovery effects using small-diameter-ratio wind turbines for vertically staggered wind farms. Journal of Renewable and Sustainable Energy, 2024, 16(4). https://doi.org/10.1063/5.0191884

[33] DARóCZY L, JANIGA G, PETRASCH K, et al. Comparative analysis of turbulence models for the aerodynamic simulation of H-Darrieus rotors. Energy, 2015, 90: 680-690.

[34] O'BRIEN J M, YOUNG T M, EARLY J M, et al. An assessment of commercial CFD turbulence models for near wake HAWT modelling . Journal of Wind Engineering and Industrial Aerodynamics, 2018, 176: 32-53.

[35] ZHU J-Y, PARK T, ISOLA P, et al. Unpaired image-to-image translation using cycle-consistent adversarial networks // Proceedings of the IEEE international conference on computer vision. Venice, Italy, 2017

[36] WANG L, XIE J, LUO W, et al. Effectiveness of data-driven wind turbine wake models developed by machine/deep learning with spatial-segmentation technique. Sustainable Energy Technologies and Assessments, 2022, 53: 102499. https://doi.org/10.1016/j.seta.2022.102499

[37] CHAMORRO L P, PORTé-AGEL F. A Wind-Tunnel Investigation of Wind-Turbine Wakes: Boundary-Layer Turbulence Effects. Boundary-Layer Meteorology, 2009, 132(1): 129-149. https://doi.org/10.1007 /s10546-009-9380-8

[38] James G, Witten D, Hastie T, Tibshirani R. An introduction to statistical learning.Springer; 2013.

[39] BARTL J, SæTRAN L. Blind test comparison of the performance and wake flow between two in-line wind turbines exposed to different turbulent inflow conditions. Wind Energy Sci, 2017, 2(1): 55-76. https://doi.org /10.5194/wes-2-55-2017

[40] SOESANTO Q M B, YOSHINAGA T, IIDA A. Anisotropic double-Gaussian analytical wake model for an isolated horizontal-axis wind turbine. Energy Science & Engineering, 2022, 10(7): 2123-2145.

[41] WU Y-T, PORTé-AGEL F. Modeling turbine wakes and power losses within a wind farm using LES: An application to the Horns Rev offshore wind farm. Renewable Energy, 2015, 75: 945-955. https://doi.org/10.1016/j.renene.2014.06.019

[42] BARTHELMIE R J, HANSEN K, FRANDSEN S T, et al. Modelling and measuring flow and wind turbine wakes in large wind farms offshore. Wind Energy, 2009, 12(5): 431-444. https://doi.org/10.1002/we.348

[43] PORTé-AGEL F, WU Y-T, CHEN C-H. A Numerical Study of the Effects of Wind Direction on Turbine Wakes and Power Losses in a Large Wind Farm. Energies, 2013, 6(10): 5297-5313. https://doi.org /10.3390/en6105297

[44] ONEL H C, TUNCER I H. Investigation of wind turbine wakes and wake recovery in a tandem configuration

using actuator line model with LES. Computers & Fluids, 2021, 220: 104872. https://doi.org/10.1016/j.compfluid.2021.104872

[45] CHEN J, ZHANG Y, XU Z, et al. Flow characteristics analysis and power comparison for two novel types of vertically staggered wind farms. Energy, 2023, 263: 126141. https://doi.org/10.1016/j.energy.2022.126141

[46] MIAO W, LI C, PAVESI G, et al. Investigation of wake characteristics of a yawed HAWT and its impacts on the inline downstream wind turbine using unsteady CFD. Journal of Wind Engineering and Industrial Aerodynamics, 2017, 168: 60-71. https://doi.org/10.1016/j.jweia.2017.05.002

[47] SHAO Y, SU J, TU Y, et al. Assessment of the aerodynamic benefits of collocating horizontal- and vertical-axis wind turbines in tandem using actuator line model. Physics of Fluids, 2023, 35(7), 075115. https://doi.org/10.1063/5.0156543

[48] CHOI N J, HYUN NAM S, HYUN JEONG J, et al. Numerical study on the horizontal axis turbines arrangement in a wind farm: Effect of separation distance on the turbine aerodynamic power output. Journal of Wind Engineering and Industrial Aerodynamics, 2013, 117: 11-17. https://doi.org/10.1016/j.jweia.2013.04.005